Raman Microspectroscopic Analysis of Changes in the Chemical Structure and Reactivity of Soot in a Diesel Exhaust Aftertreatment Model System

ARTICLE *in* ENVIRONMENTAL SCIENCE AND TECHNOLOGY · JUNE 2007

Impact Factor: 5.33 · DOI: 10.1021/es0612448 · Source: PubMed

5 AUTHORS, INCLUDING:

Armin Messerer
Mahle
17 PUBLICATIONS **422** CITATIONS
SEE PROFILE

Reinhard Niessner
Technische Universität München
595 PUBLICATIONS **12,260** CITATIONS
SEE PROFILE

Ulrich Pöschl
Max Planck Institute for Chemistry
333 PUBLICATIONS **10,035** CITATIONS
SEE PROFILE

Raman Microspectroscopic Analysis of Changes in the Chemical Structure and Reactivity of Soot in a Diesel Exhaust Aftertreatment Model System

NATALIA P. IVLEVA,* ARMIN MESSERER,† XIN YANG, REINHARD NIESSNER, AND ULRICH PÖSCHL‡

Technical University of Munich, Institute of Hydrochemistry, Marchioninistrasse 17, D-81377 Munich, Germany

Raman microspectroscopy has been applied to follow structural changes in spark discharge (GfG) soot and light-duty diesel vehicle (LDV) soot upon oxidation and gasification by nitrogen oxides and oxygen in a diesel exhaust aftertreatment model system at 523 and 573 K. Raman spectra have been recorded before and during the oxidation process, and spectral parameters have been determined by curve fitting with five bands (G, D1−D4). For GfG soot, a steep initial decrease of the relative intensity of the D3 band suggested rapid preferential oxidation of a highly reactive amorphous carbon fraction, while a less steep but also substantial decrease of band widths (in particular, the D1 band) indicated a slower overall increase of chemical homogeneity and structural order in the partially oxidized material. The spectroscopic changes are in agreement with a strong decrease of chemical reactivity at increasing mass conversion of GfG soot. In contrast, the spectral parameters and reactivity of partially oxidized LDV soot remained largely unchanged throughout the oxidation process. Overall, the spectroscopic and kinetic findings suggest that Raman spectroscopic parameters provide information about the relative abundance and structural order of graphitelike and amorphous carbon and can be used as proxies for the chemical reactivity of soot undergoing oxidation and gasification. Thus, Raman spectroscopy promises to become an efficient tool for further investigation and optimization of diesel exhaust aftertreatment in continuously regenerating traps and particle filters.

1. Introduction

Soot particles are hazardous environmental pollutants that account for a major fraction of fine air particulate matter in urban areas. They can cause and enhance respiratory, cardiovascular, and allergic diseases, and they influence atmospheric chemistry, physics, and climate (*1*−*3*).

Present and future emission limits require that soot particles are efficiently removed from diesel engine exhaust. The continuously regenerating traps (CRT) or diesel particulate filters (DPF) applied for this purpose have to be regenerated by oxidation and gasification of deposited soot (*4*−*6*). The environmental and health effects as well as the oxidation of soot are strongly influenced by the structure and size of the particles (*6*−*10*).

Soot consists mostly of carbon and is composed of agglomerated primary particles with diameters of 10−30 nm that comprise nanocrystalline (*8*, *11*−*14*) and amorphous domains. The amorphous domains are disordered mixtures of polycyclic aromatic hydrocarbons (PAH) and other organic and inorganic components (*8*, *11*, *15*, *16*). The chemical composition and structure of primary particles and agglomerates depend on the origin and conditioning of soot (*7*, *8*, *11*, *17*).

Raman spectroscopy provides fingerprint spectra which allow the distinction of a wide range of chemical substances (*11*, *18*, *19*). For the characterization of graphitelike carbon in diesel soot, it was first applied by Rosen and Novakov (*20*). Since then, several studies have reported and discussed the correlation of Raman spectroscopic parameters such as peak positions, widths, and intensity ratios with the structure of soot and related carbonaceous materials (*11*, *15*−*17*, *21*−*38*) as detailed in the Supporting Information (SI, section S1).

Here, we are following up on recent studies of the applicability of Raman microspectroscopy for structural characterization of soot (*11*) and of the kinetics of soot oxidation and gasification by nitrogen oxides and oxygen (*6*). We demonstrate the potential of Raman microspectroscopy for the analysis of changes in the chemical structure and reactivity of different types of soot during the oxidation and gasification in a diesel exhaust aftertreatment model system under conditions relevant for CRT and DPF (*6*, *39*−*42*).

2. Methods

The two types of soot investigated in this study are real diesel soot from a light-duty vehicle (LDV) operating under idling conditions and soot from a graphite spark discharge generator (GfG) (*6*, *42*−*46*). Soot oxidation experiments with nitrogen oxides and oxygen have been performed in a diesel exhaust aftertreatment model system at 523 and 573 K. Raman spectra have been recorded before and during the oxidation process with a Raman microscope system using the laser wavelength $\lambda_0 = 514$ nm. Spectral parameters have been determined by curve fitting with five bands (G, D1−D4) as proposed by Sadezky et al. (*11*). A detailed description of the oxidation experiments and Raman microspectroscopic analysis is given in the SI (section S2).

3. Results and Discussion

3.1. Raman Spectra of Fresh GfG and LDV Soot. Figure 1 shows typical examples of the spectra of fresh, untreated GfG spark discharge soot and LDV diesel soot samples, which are similar to those of other types of soot and related carbonaceous materials (*11*, *15*, *17*). All spectra recorded and evaluated in the present study have been analyzed with the five band-fitting procedures proposed by Sadezky et al. (*11*) as detailed in the SI (section S2.2).

The mean values and standard deviations of the band parameters determined from the spectra of fresh GfG and LDV soot samples are summarized in the SI (Tables S1 and S2): band position (Stokes shift, cm^{-1}), full width at half-maximum (FWHM, cm^{-1}), and integrated band intensity

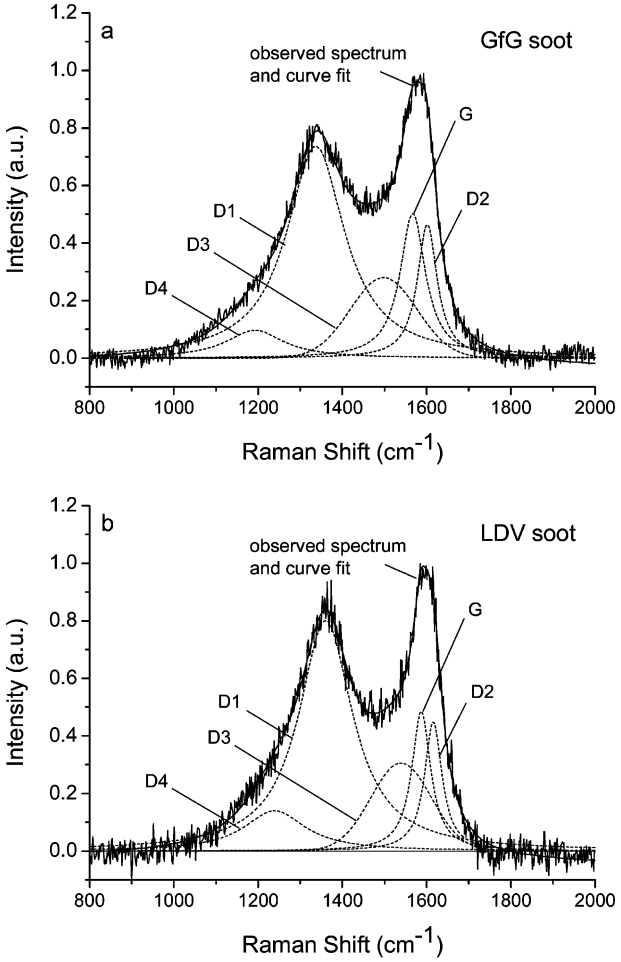

FIGURE 1. Exemplary spectra ($\lambda_0 = 514$ nm) of untreated GfG soot (a) and LDV soot (b) with five band fits (dotted lines) as proposed by Sadezky et al. (*11*).

relative to the G band (I/I_G) for four Lorentzian bands (G, D1, D2, D4) and one Gaussian band (D3).

The band widths of GfG soot (70−210 cm^{-1}) were larger than those of LDV soot (60−180 cm^{-1}), indicating a lower degree of structural order. The most pronounced differences were observed for the relative intensity of the D3 band (I_{D3}/I_G), which was by a factor of 2 higher for GfG soot than for LDV soot, suggesting a higher proportion of amorphous carbon in GfG soot.

3.2. Evolution of Raman Spectra upon Oxidation. Figure 2 shows the evolution of the spectra (averages of six to seven measurements) of GfG and LDV soot at different steps of the oxidation process, that is, after reaction times ranging from 0 to 480 min at 523 or 573 K. The peaks in the spectra of GfG soot narrowed and reversed their relative intensities with increasing reaction time, whereas the spectra of LDV soot remained largely unchanged. The corresponding spectral parameters are listed in the SI (Tables S1 and S2).

For GfG soot undergoing oxidation at 523 K, the positions (Stokes shifts) of the D1 and D3 bands remained essentially unchanged (Figure 2a and SI, Table S1a). In contrast, the Raman shifts of the G and D2 bands exhibited an increase, corresponding to a pronounced move of the overall peak maximum from ∼1580 cm^{-1} for fresh soot to ∼1610 cm^{-1} for highly oxidized soot. The fit value for the position of the D4 band exhibited a move from ∼1180 cm^{-1} for fresh soot to ∼1120 cm^{-1} for oxidized soot, which is due to the appearance of a sharp new peak at ∼1120 cm^{-1} in the spectra of oxidized GfG soot, as discussed below. For all bands, the FWHM exhibited a pronounced decrease with increasing reaction

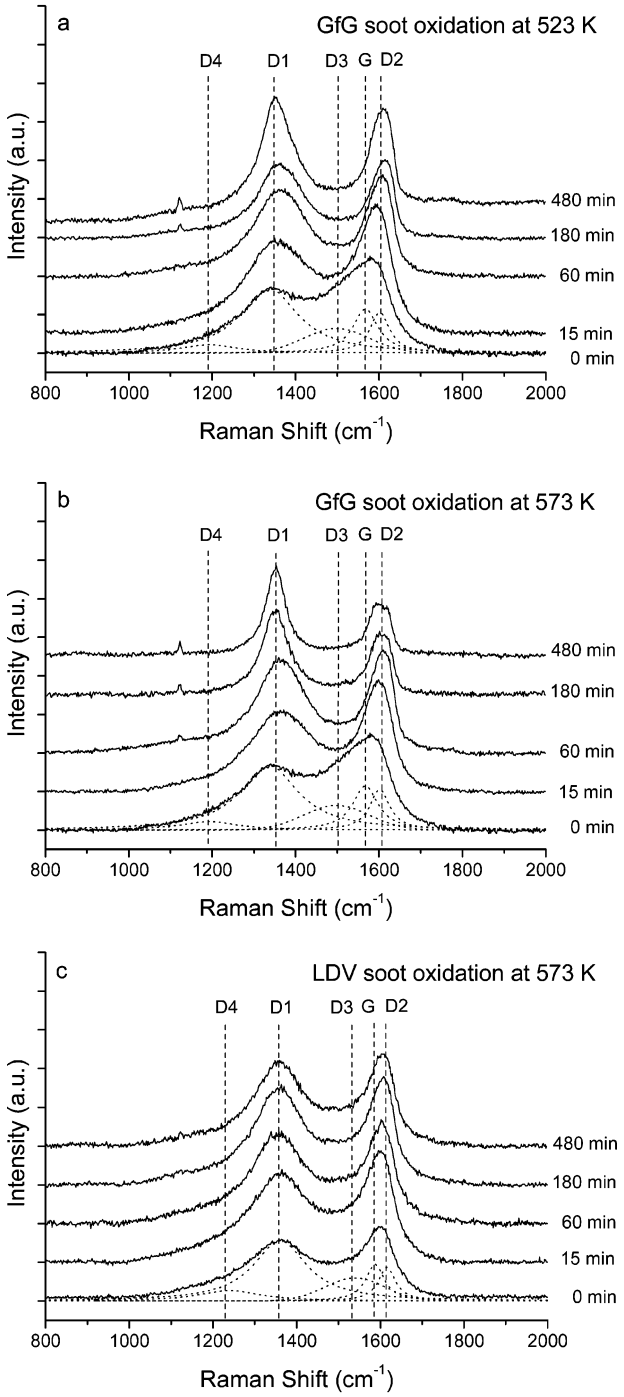

FIGURE 2. Spectra ($\lambda_0 = 514$ nm) of untreated and partially oxidized GfG soot after different reactions times at 523 K (a) and 573 K (b) and LDV soot at 573 K (c). The spectra have offsets for clarity; five band fits and band positions are illustrated by dashed and dotted lines, respectively.

time, indicating an increase of structural order and decrease of chemical heterogeneity in GfG soot undergoing oxidation. After 480 min, the FWHM's were lower by factors of ∼1.5 for G and D2, more than 2 for D1, and about 7 for D3 and D4 bands.

Upon oxidation, the intensity ratios between the G, D1, and D2 bands remained essentially unchanged, indicating near-constant proportions of carbon atoms in the bulk, at the surface, and at the edges of disturbed graphitic lattice structures (*11*, *35*). In contrast, the relative intensity of the D3 band steeply decreased with increasing reaction time, suggesting a strong decrease of the amorphous carbon

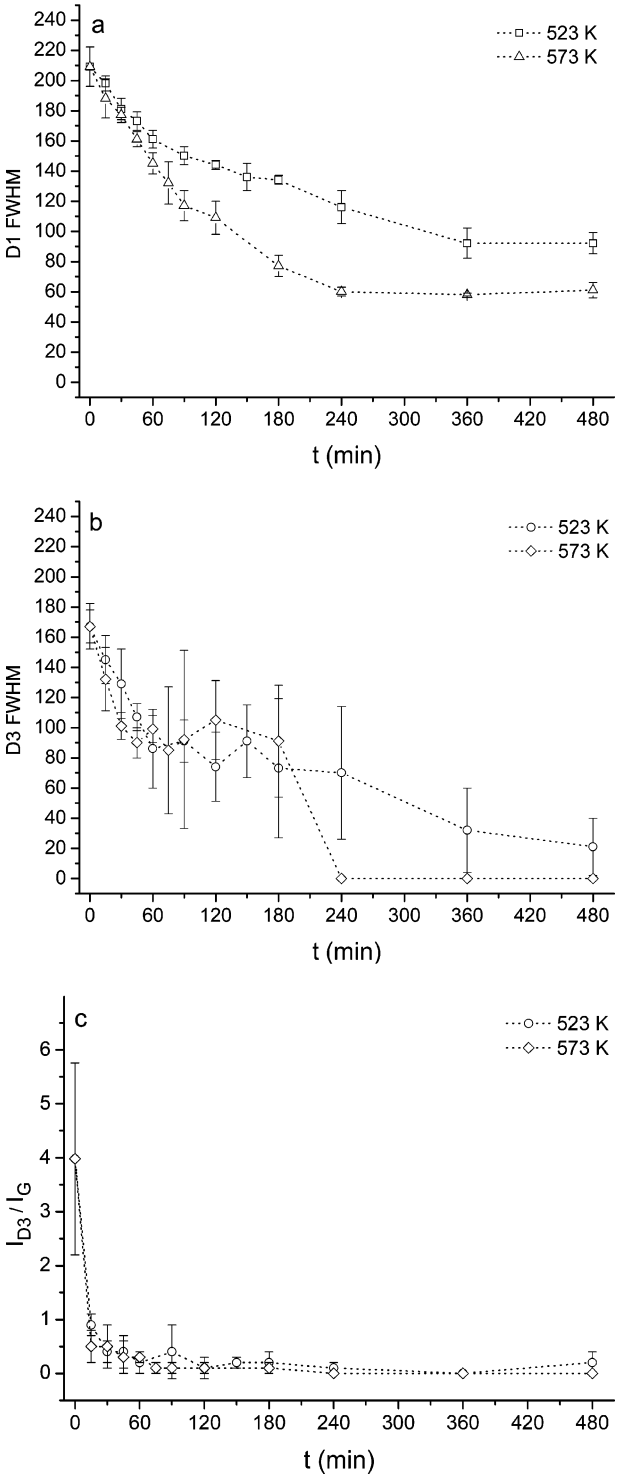

FIGURE 3. Temporal changes in FWHM of D1 (a) and D3 (b) bands and in ratio I_{D3}/I_G (c) during GfG soot oxidation at 523 and 573 K.

fraction. After 480 min of oxidation at 523 K, the ratio I_{D3}/I_G was by a factor of ~10 lower than for the fresh GfG soot. For comparison with earlier studies (*11*, *29*), we have also calculated the parameters R2 = $I_{D1}/(I_G + I_{D1} + I_{D2})$ and R3 = $I_{D3}/(I_G + I_{D2} + I_{D3})$. The parameter R2 (SI, Figure S1) showed no significant changes during oxidation (differences < standard deviations), whereas R3 exhibited a pronounced decrease similar to that of I_{D3}/I_G.

The spectra of GfG soot subject to oxidation at 573 K undergo a similar evolution as described above for 523 K (Figure 2b) but within shorter reaction times and to a larger

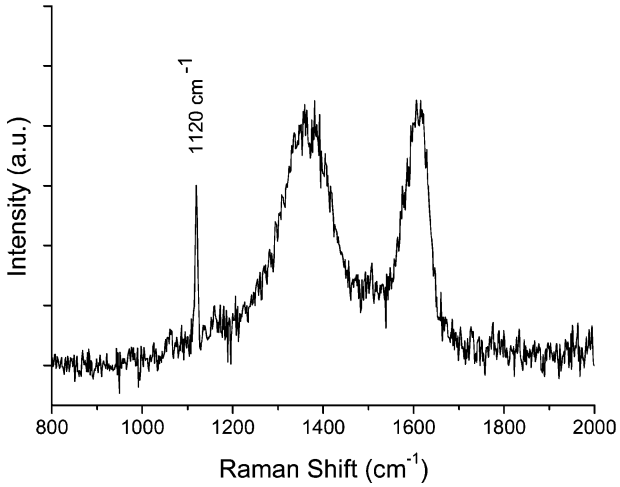

FIGURE 4. The spectrum ($\lambda_0 = 514$ nm) recorded at one of the light spots on a partially oxidized GfG soot particle agglomerate after 75 min reaction time at 573 K.

extent. After 480 min at 573 K, the D1 bandwidth was 30% lower than at 523 K, and the D3 band disappeared (curve fitting revealed no characteristic band at ~1500 cm^{-1} and thus the D3 intensity and FWHM were set to zero).

Figure 3 illustrates the temporal evolution of D1 and D3 band widths and I_{D3}/I_G upon oxidation of GfG soot at 523 and 573 K. At both temperatures, the steep initial decrease of I_{D3}/I_G suggests rapid oxidation amorphous carbon fraction, while the less steep decrease of band widths indicates a slower overall increase of chemical homogeneity and structural order in the soot samples. At 523 K, the transformation was slower and continued throughout the experiment (480 min), whereas near-constant final parameter values were reached after 240 min at 573 K.

After reaction times $t \geq 120$ min at 523 K and $t \geq 60$ min at 573 K, respectively, the spectra of the GfG soot samples exhibited an additional peak at ~1120 cm^{-1} (Figure 4). The relative intensity of the signal at ~1120 cm^{-1} was highly variable, and it was most pronounced when the laser beam was focused onto the bright spots that were observed on the sample surface (SI, Figure S2). Previously, Raman signals at 1100−1150 cm^{-1} have been associated with amorphous carbon films free of hydrogen (*47*, *48*), tetrahedral amorphous carbon films (*49*), and diamondlike carbon films (*50*). In most studies, these signals have been assigned to vibrations of sp^3-hybridized C−C bonds (*47*−*50*). Recently, however, Birrell et al. (*51*) have proposed that the band at ~1120 cm^{-1} in the spectra of ultrananocrystalline diamond could be due to carbon−hydrogen bonds at the grain boundaries. The appearance of the peak at ~1120 cm^{-1} in investigated samples suggests that heating and partial oxidation of GfG soot may lead to the formation or exposure of domains with a high content of sp^3−hybridized carbon. This aspect requires further investigation. It may become highly relevant for the design and optimization of aftertreatment systems for modern diesel engines emitting soot particles with highly disordered fullerene-like chemical structures similar to those of GfG soot.

In contrast to GfG soot, the spectra of LDV soot hardly changed upon oxidation, that is, the differences hardly exceeded the standard deviations (Figure 2c and SI, Table S2). This is consistent with the lower initial oxidation rates and slower mass conversion observed for LDV soot compared to GfG soot. After 480 min at 573 K, the D1 bandwidth was only ~15% lower than the initial value, and I_{D3}/I_G decreased by a factor of ~2 but the difference was not larger than the standard deviation of the initial value. At 523 K, no significant changes were observed in the spectra.

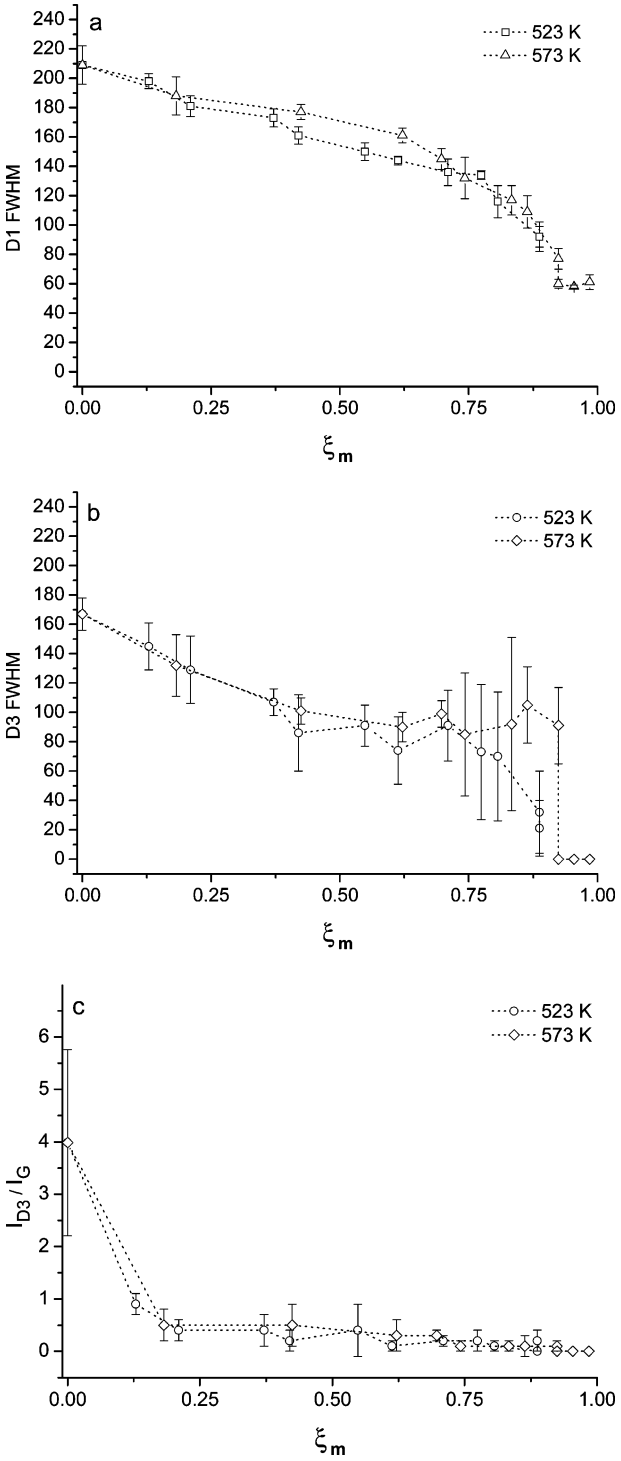

FIGURE 5. FWHM of D1 (a) and D3 (b) bands and ratio I_{D3}/I_G (c) vs mass conversion ξ_m during GfG soot oxidation at 523 and 573 K.

3.3. Mass Conversion and Change of Spectral Parameters. In Figure 5, the spectral parameters which exhibited the most pronounced and consistent change upon oxidation of GfG soot (the D1 and D3 bandwidths and the ratio I_{D3}/I_G) are plotted against the mass conversion of the investigated samples as determined by gravimetry.

The plots demonstrate very good agreement between the data sets obtained from the oxidation experiments performed at 523 and 573 K, indicating high reproducibility and reliability of the measurement and fitting procedures. The near-identical dependence of the spectral parameters on ξ_m suggests that the observed changes in the spectra are

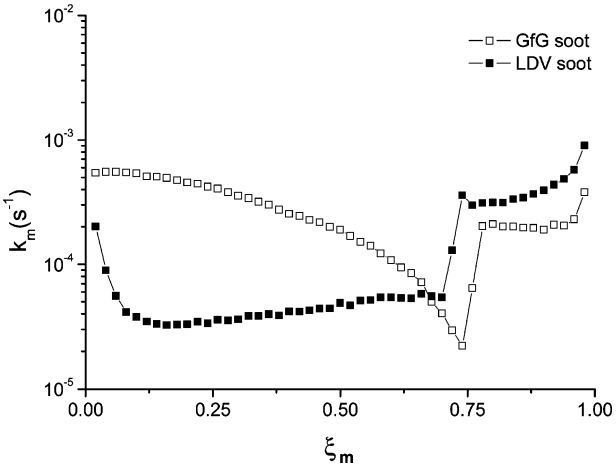

FIGURE 6. Carbon pseudo-first-order rate coefficient k_m vs mass conversion ξ_m for GfG and LDV soot oxidation experiments at 598 K. Sudden increase at $\xi_m = 0.7$ is due to temperature increase to 673 K (*6*).

primarily due to the preferential oxidation and removal of the highly reactive amorphous carbon fraction of GfG soot. Apparently, structural changes inside the residual material (graphitic lattice structures) are less important for the temporal evolution of the spectra upon oxidation of GfG soot. This is consistent with the near-constant intensity ratios between the bands related to graphitic lattice structures (G, D1, and D2) as discussed above.

The steep initial decrease of I_{D3}/I_G from ~4 at $\xi_m = 0$ to less than 0.5 at $\xi_m \approx 0.2$ (Figure 5c) suggests that ~20% of the mass of fresh GfG soot consists of highly reactive amorphous carbon, which is rapidly oxidized and gasified upon exposure to NO_2. On the other hand, the decrease of the D1 bandwidth of GfG soot from an initial value of ~210 cm^{-1} to values smaller than that of LDV soot (~150 cm^{-1}) at $\xi_m > 0.7$ suggests that up to ~30% of the mass of partially oxidized GfG soot consists of graphitic carbon with a higher degree of order and less chemical heterogeneity than that of LDV soot. This is consistent with the results of earlier investigations of the reactivity of GfG and LDV soot under engine exhaust conditions (*6*).

Figure 6 shows the carbon-mass-based pseudo-first-order rate coefficients (k_m) for the oxidation and gasification of GfG and LDV soot at 598 K determined as described by Messerer et al. (*6*) and plotted against mass conversion. At low mass conversion, the reaction rate coefficients of GfG soot are up to 1 order of magnitude higher, but they drop below those of LDV soot at $\xi_m > 0.7$. Moreover, the dependence of the D1 bandwidth of GfG soot on ξ_m exhibits a similar curvature as the dependence of k_m on ξ_m. LDV soot, on the other hand, exhibits only minor variations of D1 bandwidth (SI, Figure S3) and near-constant reactivity (Figure 6). The initial decrease of k_m can be attributed to the decomposition of surface functional groups, and the subsequent increase can be explained by an increase of surface-to-volume ratio (*6*). Overall, the observations suggest that the D1 bandwidth does not only characterize the degree of order of graphitic carbon but can also be used as a proxy for the reactivity of soot toward oxidation and gasification.

3.4. Implications and Outlook. Recent electron microscopic investigations (*7*, *8*) have shown that differences in the oxidation behavior of different types of soot are associated with the different microstructures. GfG soot as well as diesel soot from modern heavy-duty diesel engines (EuroIV) is characterized by highly disordered fullerene-like structures and are oxidized faster than the well-graphitized soot samples (black smoke soot and carbon black). Vander Wal et al. (*22*)

found close correlations between Raman spectroscopic parameters and the results of lattice fringe analysis of high-resolution electron microscopy (HRTEM) images recorded upon graphitization of amorphous carbon black. Fang and Lance (*32*) have reported that Raman spectroscopy can be used to study the influence of tempering on the structure and reactivity of soot and the regeneration of DPF.

Our results demonstrate that Raman microspectroscopy can be used to investigate changes in the structure and reactivity of soot also upon oxidation and gasification under conditions relevant for CRT and DPF. A detailed elucidation of molecular and crystalline structures and their relation to the reactivity and Raman spectroscopic parameters of soot will require further comprehensive studies combining kinetic experiments, Raman spectroscopy, and HRTEM. Beyond lab- and cost-intensive fundamental research, however, Raman spectroscopy promises to become a particularly efficient tool for the design and optimization of diesel exhaust aftertreatment systems. This may become increasingly important if the development of modern diesel engines makes soot particles smaller and more reactive but also more susceptible to structural rearrangements and passivation (*10*).

Acknowledgments

Financial support by BFS (project "Development of a catalytic system for the continuous reduction of soot particle emissions of HDV diesel engines") and by BMBF (AFO2000, CARBAERO, 07ATC05) is gratefully acknowledged.

Supporting Information Available

Additional information about Raman spectra of soot, experimental details, and complementary tables and figures are reported. This material is available free of charge via the Internet at http://pubs.acs.org.

Literature Cited

(1) Sydbom, A.; Blomberg, A.; Parnia, S.; Stenfors, N.; Sandstrom, T.; Dahlen, S. E. Health effects of diesel exhaust emissions. *Eur. Respir. J.* **2001**, *17*, 733−746.

(2) Pöschl, U.; Letzel, T.; Schauer, C.; Niessner, R. Interaction of ozone and water vapor with spark discharge soot aerosol particles coated with benzo[a]pyrene: O_3 and H_2O adsorption, benzo[a]pyrene degradation, and atmospheric implications. *J. Phys. Chem. A* **2001**, *105*, 4029−4041.

(3) Pöschl, U. Atmospheric aerosols: composition, transformation, climate and health effects. *Angew. Chem., Int. Ed.* **2005**, *44*, 7520−7540.

(4) Saracco, G.; Badini, C.; Specchia, V. Catalytic traps for diesel particulate control. *Chem. Eng. Sci.* **1999**, *54*, 3035−3041.

(5) Messerer, A.; Rothe, D.; Pöschl, U.; Niessner, R. Advances in the development of filterless soot deposition systems for the continuous removal of diesel particulate matter. *Top. Catal.* **2004**, *30*/*31*, 247−250.

(6) Messerer, A.; Niessner, R.; Pöschl, U. Comprehensive kinetic characterization of the oxidation and gasification of model and real diesel soot by nitrogen oxides and oxygen under engine exhaust conditions: measurement, Langmuir-Hinshelwood, and Arrhenius parameters. *Carbon* **2006**, *44*, 307−324.

(7) Müller, J. O.; Su, D. S.; Jentoft, R. E.; Wild, U.; Schlögl, R. Diesel engine exhaust emission: Oxidative behavior and microstructure of black smoke soot particulate. *Environ. Sci. Technol.* **2006**, *40*, 1231−1236.

(8) Su, D. S.; Jentoft, R. E.; Müller, J. O.; Rothe, D.; Jacob, E.; Simpson, C. D.; Tomovic, Z.; Müllen, K.; Messerer, A.; Pöschl, U.; Niessner, R.; Schlögl, R. Microstructure and oxidation behaviour of Euro IV diesel engine soot: a comparative study with synthetic model soot substances. *Catal. Today* **2004**, *90*, 127−132.

(9) Higgins, K. J.; Jung, H.; Kittelson, D. B.; Roberts, J. T.; Zachariah, M. R. Size-selected nanoparticle chemistry: Kinetics of soot oxidation. *J. Phys. Chem. A* **2002**, *106*, 96−103.

(10) Su, D. S.; Müller, J. O.; Jentoft, R. E.; Rothe, D.; Jacob, E.; Schlögl, R. Fullerene-like soot from EuroIV diesel engine: Consequences for catalytic automotive pollution control. *Top. Catal.* **2004**, *30/31*, 241−245.

(11) Sadezky, A.; Muckenhuber, H.; Grothe, H.; Niessner, R.; Pöschl, U. Raman spectra of soot and related carbonaceous materials: Spectral analysis and structural information. *Carbon* **2005**, *43*, 1731−1742.

(12) Müller, J. O.; Su, D. S.; Jentoft, R. E.; Kröhnert, J.; Jentoft, F. C.; Schlögl, R. Morphology-controlled reactivity of carbonaceous materials towards oxidation. *Catal. Today* **2005**, *102/103*, 259−265.

(13) Homann, K.-H. Fullerenes and soot formation - New pathways to large particles in flames. *Angew. Chem., Int. Ed.* **1998**, *37*, 2435−2451.

(14) Oberlin, A. High-resolution TEM studies of carbonization and graphitization. *Chem. Phys. Carbon* **1989**, *22*, 1−143.

(15) Sze, S.-K.; Siddique, N.; Sloan, J. J.; Escribano, R. Raman spectroscopic characterization of carbonaceous aerosols. *Atmos. Environ.* **2001**, *35*, 561−568.

(16) Ferrari, A. C.; Robertson, J. Interpretation of Raman spectra of disordered and amorphous carbon. *Phys. Rev. B: Condens. Matter Mater. Phys.* **2000**, *61*, 14095−14107.

(17) Dippel, B.; Jander, H.; Heintzenberg, J. NIR FT Raman spectroscopic study of flame soot. *Phys. Chem. Chem. Phys.* **1999**, *1*, 4707−4712.

(18) McCreery, R. L. Magnitude of Raman scattering. In *Raman Spectroscopy for Chemical Analysis*; Winefordner, J. D., Ed.; John Wiley & Sons: New York, 2000; Vol. 157, pp 15−35.

(19) Ivleva, N. P.; Niessner, R.; Panne, U. Characterization and discrimination of pollen by Raman microscopy. *Anal. Bioanal. Chem.* **2005**, *381*, 261−267.

(20) Rosen, N.; Novakov, T. Raman scattering and characterisation of atmospheric aerosol particles. *Nature* **1977**, *266*, 708−710.

(21) Escribano, R.; Sloan, J. J.; Siddique, N.; Sze, N.; Dudev, T. Raman spectroscopy of carbon-containing particles. *Vib. Spectrosc.* **2001**, *26*, 179−186.

(22) Vander Wal, R. L.; Tomasek, A. J.; Street, K.; Hull, D. R.; Thompson, W. K. Carbon nanostructure examinated by Lattice Fringe Analysis of High-Resolution Transmission Electron Microscopy. *Appl. Spectrosc.* **2004**, *58*, 230−237.

(23) Van Doorn, J.; Vuurman, M. A.; Tromp, P. J. J.; Stufkens, D. J.; Moulijn, J. A. Correlation between Raman spectroscopic data and the temperature-programmed oxidation reactivity of coals and carbons. *Fuel Process. Technol.* **1990**, *24*, 407−413.

(24) Tuinstra, F.; Koenig, J. L. Raman spectrum of graphite. *J. Chem. Phys.* **1970**, *53*, 1126−1130.

(25) Dresselhaus, M. S.; Dresselhaus, G.; Saito, R.; Jorio, A. Raman spectroscopy of carbon nanotubes. *Phys. Rep.* **2005**, *409*, 47−99.

(26) Sood, A. K.; Gupta, R.; Asher, S. A. Origin of the unusual dependence of Raman D band on excitation wavelength in graphite-like materials. *J. Appl. Phys.* **2001**, *90*, 4494−4497.

(27) Sood, A. K.; Gupta, R.; Asher, S. A. Erratum: Origin of the unusual dependence of Raman D band on excitation wavelength in graphite-like materials. *J. Appl. Phys.* **2001**, *90*, 4494; *J. Appl. Phys.* **2002**, *91*, 547.

(28) Jawhari, T.; Roid, A.; Casado, J. Raman spectroscopic characterization of some commercially available carbon black materials. *Carbon* **1995**, *33*, 1561−1565.

(29) Beyssac, O.; Goffe, B.; Petitet, J.-P.; Froigneux, E.; Moreau, M.; Rouzaud, J.-N. On the characterization of disordered and heterogeneous carbonaceous materials by Raman spectroscopy. *Spectrochim. Acta, Part A* **2003**, *59A*, 2267−2276.

(30) Cuesta, A.; Dhamelincourt, P.; Laureyns, J.; Martinez-Alonso, A.; Tascon, J. M. D. Raman microprobe studies on carbon materials. *Carbon* **1994**, *32*, 1523−1532.

(31) Gruber, T.; Zerda, T. W.; Gerspacher, M. Raman studies of heat-treated carbon blacks. *Carbon* **1994**, *32*, 1377−1382.

(32) Fang, H. L.; Lance, M. J. Influence of soot surface changes on DPF regeneration. *Soc. Automot. Eng., SP* **2004**, *SP−1898*, 89−97.

(33) Thomsen, C.; Reich, S. Double resonant Raman scattering in graphite. *Phys. Rev. Lett.* **2000**, *85*, 5214−5217.

(34) Matthews, M. J.; Pimenta, M. A.; Dresselhaus, G.; Dresselhaus, M. S.; Endo, M. Origin of dispersive effects of the Raman D band in carbon materials. *Phys. Rev. B: Condens. Matter Mater. Phys.* **1999**, *59*, R6585−R6588.

(35) Wang, Y.; Alsmeyer, D. C.; McCreery, R. L. Raman spectroscopy of carbon materials: structural basis of observed spectra. *Chem. Mater.* **1990**, *2*, 557−563.

(36) Cancado, L. G.; Pimenta, M. A.; Saito, R.; Jorio, A.; Ladeira, L. O.; Grueneis, A.; Souza-Filho, A. G.; Dresselhaus, G.; Dresselhaus, M. S. Stokes and anti-Stokes double resonance Raman scattering in two-dimensional graphite. *Phys. Rev. B: Condens. Matter Mater. Phys.* **2002**, *66*, 035415/035411−035415/035415.

(37) Livneh, T.; Haslett, T. L.; Moskovits, M. Distinguishing disorder-induced bands from allowed Raman bands in graphite. *Phys. Rev. B: Condens. Matter Mater. Phys.* **2002**, *66*, 195110/195111−195110/195111.
(38) Vidano, R. P.; Fischbach, D. B.; Willis, L. J.; Loehr, T. M. Observation of Raman band shifting with excitation wavelength for carbons and graphites. *Solid State Commun.* **1981**, *39*, 341−344.
(39) Messerer, A.; Rothe, D.; Niessner, R.; Pöschl, U. Kinetic considerations and model calculations for continuous regeneration of commercial vehicle engines-diesel soot particle separation systems. *Chem. Ing. Tech.* **2005**, *77*, 881−886.
(40) Setiabudi, A.; Makkee, M.; Moulijn, J. A. The role of NO_2 and O_2 in the accelerated combustion of soot in diesel exhaust gases. *Appl. Catal., B* **2004**, *50*, 185−194.
(41) Kandylas, I. P.; Koltsakis, G. C. NO_2-assisted regeneration of diesel particulate filters: A modeling study. *Ind. Eng. Chem. Res.* **2002**, *41*, 2115−2123.
(42) Hackfort, H.; Hunnekes, E.; Dornseiffer, J. Fundamental investigations of continuous regeneration of carbon particle traps with oxygen. *Soc. Automot. Eng., SP* **2000**, *SP−1561*, 179−184.
(43) Kamm, S.; Saathoff, H.; Naumann, K. H.; Moehler, O.; Schurath, U. Gasification of a soot aerosol by O_3 and NO_2: Temperature dependence of the reaction probability. *Combust. Flame* **2004**, *138*, 353−361.
(44) Helsper, C.; Moelter, W.; Loeffler, F.; Wadenpohl, C.; Kaufmann, S.; Wenninger, G. Investigations of a new aerosol generator for the production of carbon aggregate particles. *Atmos. Environ., Part A* **1993**, *27A*, 1271−1275.
(45) Wentzel, M.; Gorzawski, H.; Naumann, K. H.; Saathoff, H.; Weinbruch, S. Transmission electron microscopical and aerosol dynamical characterization of soot aerosols. *J. Aerosol Sci.* **2003**, *34*, 1347−1370.
(46) Evans, D. E.; Harrison, R. M.; Ayres, J. G. The generation and characterization of elemental carbon aerosols for human challenge studies. *J. Aerosol Sci.* **2003**, *34*, 1023−1041.
(47) Logothetidis, S. Hydrogen-free amorphous carbon films approaching diamond prepared by magnetron sputtering. *Appl. Phys. Lett.* **1996**, *69*, 158−160.
(48) Logothetidis, S.; Gioti, M.; Lioutas, C. New forms of hydrogen-free amorphous carbon films. *Carbon* **1998**, *36*, 539−543.
(49) Paillard, V. On the origin of the 1100 cm^{-1} Raman band in amorphous and nanocrystalline sp^3 carbon. *Europhys. Lett.* **2001**, *54*, 194−198.
(50) Paillard, V.; Melinon, P.; Dupuis, V.; Perez, J. P.; Perez, A.; Champagnon, B. Diamondlike carbon films obtained by low energy cluster beam deposition: evidence of a memory effect of the properties of free carbon clusters. *Phys. Rev. Lett.* **1993**, *71*, 4170−4173.
(51) Birrell, J.; Gerbi, J. E.; Auciello, O.; Gibson, J. M.; Johnson, J.; Carlisle, J. A. Interpretation of the Raman spectra of ultrananocrystalline diamond. *Diamond Relat. Mater.* **2005**, *14*, 86−92.

Received for review May 24, 2006. Revised manuscript received November 3, 2006. Accepted February 27, 2007.

ES0612448